Applied Surface Science 421 (2017) 389–396

Contents lists available at ScienceDirect

Applied Surface Science

journal homepage: www.elsevier.com/locate/apsusc

Full Length Article

Composition and temperature dependent optical properties of $Al_xGa_{1-x}N$ alloy by spectroscopic ellipsometry

Yao Liu[a,b], Qing Xuan Li[a], Ling Yu Wan[a], Bahadir Kucukgok[b], Ehsan Ghafari[b], Ian T. Ferguson[c], Xiong Zhang[d], Shuchang Wang[e], Zhe Chuan Feng[a,*], Na Lu[b,*]

[a] Laboratory of Optoelectronic Materials & Detection Technology, Guangxi Key Laboratory for the Relativistic Astrophysics, School of Physical Science & Technology, Guangxi University, 530004 Nanning, China
[b] Lyles School of Civil Engineering, School of Materials Engineering, Birck Nanotechnology Center, Purdue University, West Lafayette, IN 47907, USA
[c] Department of Electrical and Computing Engineering, Missouri University of Science and Technology, MO 65409, USA
[d] School of Electronic Science and Engineering, Southeast University, 210096 Nanjing, China
[e] College of Physics and Electronic Engineering, Changshu Institute of Technology, 215500 Changshu, China

ARTICLE INFO

Article history:
Received 28 July 2016
Received in revised form 29 January 2017
Accepted 31 January 2017
Available online 2 February 2017

Keywords:
$Al_xGa_{1-x}N$
Temperature
Optical properties
Spectroscopic ellipsometry

ABSTRACT

A series of $Al_xGa_{1-x}N$/AlN/Sapphire films with x = 0.35–0.75 and different thickness of epi-layer were prepared by metalorganic chemical vapor deposition (MOCVD). Spectroscopic ellipsometry (SE) was used to study the temperature-dependent refractive indices and optical bandgaps of the $Al_xGa_{1-x}N$ films ranging from 300 to 823 K. Parametric semiconductor (PSEMI) models were used to describe the dielectric functions of AlGaN/AlN layers. The fitting results of refractive index, energy bandgap, thickness and surface roughness at 300 K are in good agreement with photoluminescence (PL), scanning electron microscopy (SEM) measurements and the existing literature. Our finding indicates that the crystal quality of the samples with x = 0.47 and 0.60 are better than those with x = 0.35 and 0.75. As the temperature rises, the increasing of refractive index for the low Al content $Al_xGa_{1-x}N$ layers is stronger than that of high Al content in the transparent region, and the reduction of bandgap with high Al content is larger than that of low Al content. For all the samples (x = 0.35–0.75), an analytical expression for temperature-dependent refractive index in the wavelength range of 195–1650 nm was obtained using the Sellmeier law, and the quantitative analysis of the SE-derived temperature-dependent bandgap was conducted by using the Bose-Einstein equation.

1. Introduction

Wide band-gap AlGaN alloys are of great interest for the development of high-temperature, high-power and deep ultraviolet (UV) optoelectronic devices, due to their high thermal conductivity, high dielectric constant and continuously tunable bandgap [1–3]. For instance, photodiodes combined with $Al_xGa_{1-x}N$ distributed Bragg reflectors (DBR) can operate at temperatures higher than 650 K [4,5]; the lattice temperature of AlGaN HEMT can exceed 700 K based on the self-heating effect for the applications of high-power switching [6]; AlGaN based gas sensor can be integrated with microwave electrodes or with UV detector and emitter at temperature range of 300–773 K [7]. For these high-temperature applications, understanding of the thermo-optic effect (dependence of the refractive index on temperature) [4] and the variation of bandgap with the function of temperature are essential to improve the material quality and device performance.

Various experiments such as transmission spectra and photoluminescence (PL) measurements have been carried out in the past to investigate the temperature-dependent optical properties of $Al_xGa_{1-x}N$ films. Brunner et al. [8] and Sohal et al. [9] reported the refractive index and bandgap of AlGaN films on low temperature (7–300 K) by using transmission spectroscopy. Watanable et al. [4] utilized optical interference measurements to evaluate the refractive index up to the temperature of 788 K for GaN and AlN, but not for AlGaN alloys. Furthermore, Nepal et al. [10] investigated the temperature-dependent bandgap energy in AlGaN epi-layers from 10 to 800 K measured by PL spectroscopy. However, PL measurement cannot investigate the thermo-optic effect. On the other hand, refractive index and band gap of III-nitrides can be accurately extracted by spectroscopic ellipsometry (SE). For instance, Tisch

* Corresponding authors.
E-mail addresses: fengzc@gxu.edu.cn, zcfeng@ntu.edu.tw (Z.C. Feng), luna@purdue.edu (N. Lu).

http://dx.doi.org/10.1016/j.apsusc.2017.01.309
0169-4332/

et al. [11] reported the refractive indices of AlGaN measured by SE from 300 to 580 K over a 248–827 nm wavelength range. The temperature-dependent optical properties of AlN and GaN have also been studied in other literature [12–15] by using ellipsometry measurements, but no more than 630 K. Up to now, few studies have been reported the impact of high temperatures (especially $T > 600$ K) on the optical constants and energy bandgap of AlGaN films by ellipsometry.

To fill this knowledge gap, this study aims to investigate the optical constants and bandgaps of $Al_xGa_{1-x}N$ films with temperatures ranging from 300 to 823 K by using a dual-rotating compensator ellipsometer. In this article, metalorganic chemical vapor deposition (MOCVD) technique was used for growing $Al_xGa_{1-x}N$/AlN/Sapphire structure with different thickness epi-layers and Al molar fractions ($0.35 \leq x \leq 0.75$).

2. Experimental methods

2.1. Film growth

The $Al_xGa_{1-x}N$ samples studied here were grown on c-plane (0001) sapphire substrates by MOCVD in a low pressure (40 Torr). Source materials were trimethyl-aluminum (TMAl), trimethyl-gallium (TMGa), and ammonia (NH_3). A nominal 12 nm-thick low-temperature (LT) AlN nucleation layer was firstly grown at 600 °C, followed with a 140 nm-thick high-temperature (HT) AlN nucleation layer grown at 1040 °C. Finally, $Al_xGa_{1-x}N$ epi-layers with different thickness were deposited at same temperature of 1040 °C. Four samples with different Al content were grown by controlling the flux of TMAl, and Al molar fractions (x = 0.35, 0.47, 0.60, 0.75) were calculated by high resolution x-ray diffraction (HRXRD) assuming Vegard's law [16], as listed in Table 1.

2.2. Spectroscopic ellipsometric measurements

SE is a non-destructive method that can precisely determine optical constants, surface roughness and thickness of layers. It is based on the measurement of the change in the polarization state psi (ψ) and delta (Δ) of light upon reflection from the surface and the interfaces, and the utilization of the appropriate dispersion models [17,18].

In this study, SE measurements were taken over a spectral range of 193–1650 nm (6.36–0.75 eV) with a step of 0.5 nm using a dual-rotating compensator ellipsometer equipped with a Linkam heating and freezing stage system (THMS600). The light source combined with a deuterium lamp and a halogen lamp provided a continuous spectrum of incidence radiation at three angles of 50°, 55° and 60°. Samples were mounted on a stress-free high temperature stage, and temperature was controlled between 300 K and 823 K with the help of a heating element wire and a water circulator. Temperatures were monitored using an embedded thermocouple placed inside the sample holder and a thermocouple placed on the top corner of the sample. The SE measurements were carried out at every elevated temperature point after setting the temperature for half to one hour, to make the temperature difference between sample holder and sample surface to be less than 10 K even at the highest temperature. Eleven temperature points were measured for each sample from 300 to 823 K and the experimental spectra were recorded according to the monitored surface temperature of samples.

Deep UV PL spectroscopy (Photon Systems Inc.) has also been employed to investigate the effect of various Al compositions on the bandgap energy of AlGaN alloys at 300 K and to compare with the results obtained by SE. The PL spectroscopy system used here consists of a HeAg laser with an excitation wavelength at 224 nm (around 5.53 eV) and a 10 Hz repetition rate, a monochromator (0.25 m), and an integrated photomultiplier (PMT) detector with a wavelength range of 224–850 nm and a resolution of 0.1 nm.

3. Modeling and fitting

A SE analysis software, namely CompleteEASE (J.A. Woollam Inc.), was used to extract every layer thickness, surface roughness and optical constants of the $Al_xGa_{1-x}N$ samples from the measured ψ and Δ spectra. A five-layer model was applied to describe the material system. Factors including the effects of substrate, AlN nucleation layer and interface layer followed by the AlGaN epi-layer and surface roughness were considered in the model. The HT-AlN and LT-AlN layers of the structure were simplified to be one nucleation layer in the model, since larger number of layers and subsequent unknown parameters could increase the correlation of fit parameters and the risk of fitting error. The interface layer was defined between the AlN nucleation layer and AlGaN epi-layer, to model the interfacial intermixing of the layers above and below in 50:50 Bruggeman effective medium approximation (EMA) [19]. The introduction of this thin interface improved the fitting quality of our samples. The surface roughness was a mixture of AlGaN/voids over-layer, also modeled by Bruggeman EMA. The dielectric function of the sapphire substrate was provided by Adachi [20], and the one of the AlN nucleation layer was described by two Parametric Semiconductor (PSEMI) oscillators (Psemi-M0 and Psemi-Tri) and one Gaussian oscillator [21]. The parameterization of the AlGaN epi-layer dielectric functions can also be performed by combining two PSEMI oscillators of Psemi-M0 and Psemi-Tri. The PSEMI models, developed by Herzinger and Johs [22,23], are allowed to vary and fit seven out of twelve free parameters in each oscillator. They have high efficiency and accuracy for fitting ε_2 (the imaginary part of dielectric function) critical point of direct bandgap crystalline semiconductor by combining a highly flexible functional shape with Kramers-Kronig integration [21].

A regression fitting algorithm was applied to vary the thickness of all the layers, along with adjusting fourteen parameters of the AlGaN epi-layer and seventeen parameters of the AlN layer, until the fitted ellipsometric parameters (ψ and Δ) of the multi-layer model matched the experimental SE data. The mean squared error lower than 4 indicates that the fitting results are in good agreement with the measured results. The uniaxial anisotropy of the hexagonal AlGaN samples was omitted in our models, since the rather weak optical anisotropy has been illustrated by several authors [11,24,25], and the difference in the fitted results of the ordinary and extraordinary refractive indices was below 0.5% for our samples when considering the anisotropy.

4. Results and discussion

4.1. Influence of Al molar fraction and thickness on optical properties at 300 K

Fig. 1 shows as an example, the experimental and the best fitting results of ellipsometric spectra for $Al_xGa_{1-x}N$ (x = 0.47) sample at 300 K, where the incident angles are 50°, 55° and 60°. The best-fit values of all the parameters in every oscillator for the AlGaN and AlN dielectric function are listed in Table 2. As we can see, the spectra displays interference oscillations below the bandgap corresponding to the transparent region of the sample, and the oscillations vanish above the bandgap due to the total absorption of the incident light by the layer. The same trends are observed in the other three studied samples.

Table 1 also shows the best-fit thicknesses of every layer by SE and the epi-layer thicknesses measured by cross-sectional scan-

Table 1
Summary of growth properties and thickness information of $Al_xGa_{1-x}N$ samples.

Al content x		0.35	0.47	0.60	0.75
Flux of TMAl (sccm)		40	40	40	40
Flux of TMGa (sccm)		9	6	4	2
Growth rate of $Al_xGa_{1-x}N$ layer (nm/min)		9.55	7.4	5.3	3.6
Nominal thickness of $Al_xGa_{1-x}N$ layer (nm)		723	592	471	371
SEM measured thickness of $Al_xGa_{1-x}N$ layer (nm)		770	594	521	364
SE fitted thicknesses	$Al_xGa_{1-x}N$ layer (nm)	775.3 ± 1.5	560.8 ± 2.7	502.1 ± 4.0	389.0 ± 2.1
	Interface layer (nm)	26.9 ± 1.3	31.2 ± 2.1	28.8 ± 3.2	41.3 ± 3.6
	AlN layers (nm)	72.3 ± 3.3	43.0 ± 1.5	40.7 ± 4.1	38.8 ± 1.8
SE fitted surface roughness (nm)		3.4 ± 0.2	2.5 ± 0.1	2.9 ± 0.1	4.8 ± 0.2

Table 2
The fit oscillator parameters in AlGaN and AlN layers for $Al_xGa_{1-x}N$ (x = 0.47) at 300 K.

Model structure		Parameter/			Value			
$Al_xGa_{1-x}N$ epi- *epi*-layer	PSEMI-M0	Amp/ 0.835 ± 0.121	Br/ 0.066 ± 0.008	E0/4.474 ± 0.011	WR/ 5.362 ± 1.593	PR/ 0.875 ± 0.117	AR/ 2.091 ± 0.424	O2R/ −1.000 ± 0.088
	PSEMI-Tri	Amp/ 29.415 ± 9.187	Br/ 1.013 ± 0.011	Ec/ 7.495 ± 0.061	WL/ 0.232 ± 0.076	WR/ 0.246 ± 0.077	AL/ 0.608 ± 0.307	AR/ 0.632 ± 0.302
AlN nucleation layer	PSEMI-M0	Amp/ 2.585 ± 0.004	Br/ 0.191 ± 0.033	E0/ 6.388 ± 0.035	WR/ 4.139 ± 0.001	PR/ 0.093 ± 0.001	AR/ 1.604 ± 0.002	O2R/ −0.185 ± 0.001
	PSEMI-Tri	Amp/ 5.022 ± 0.018	Br/ 0.527 ± 0.103	Ec/ 8.057 ± 0.141	WL/ 0.202 ± 0.007	WR/ 0.2011 ± 0.008	AL/ 0.505 ± 0.024	AR/ 0.504 ± 0.024
	Gaussian	Amp/ 0.987 ± 0.060	Br/ 0.393 ± 0.028	En/ 9.917 ± 0.604				

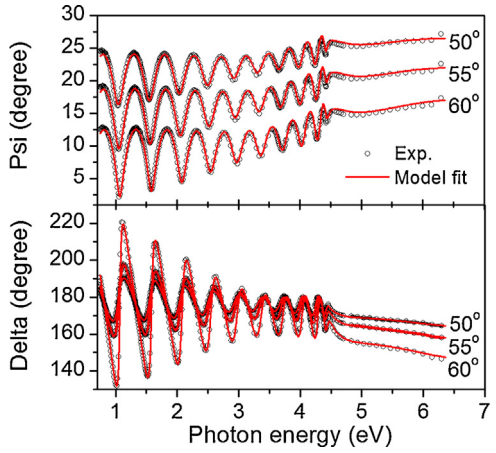

Fig. 1. SE experimental (open black circle) and fitted (solid red line) psi and delta spectra vs. photon energy of incidence (50°, 55° and 60°) for $Al_xGa_{1-x}N$ (x = 0.47) at 300 K.

ning electron microscopy (SEM). The thicknesses of AlGaN epi-layer extracted from SE fitting agree well with the values determined by SEM, and the actual thickness of AlGaN layer decreases with the increasing Al content.

The surface morphologies of the AlGaN samples were also investigated by SEM, as shown in Fig. 2. The insertion of two AlN inter-layers apply a compressive strain instead of tensile stress to the AlGaN layer and thus prevent the crack formation [26,27], due to the larger lattice constant of a = 0.3189 nm for GaN than the one of a = 0.3112 nm for AlN in (0001) plane [28]. Therefore, SEM images exhibit smooth and homogeneous surfaces in samples with Al content x = 0.47 and 0.60. As the Al content is decreased to 0.35, some small dots were observed in the surface, which can be associated with the enhanced compressive strain in the AlGaN layer due to the thicker epi-layer (listed in Table 1) and larger lattice mismatch between AlGaN and AlN layers in samples with lower Al content of 0.35. At the highest Al content x = 0.75, many pits spread over the entire surface of the sample. This phenomenon can be attributed to the strong adhesion and low surface mobility of Al atoms and insufficient growth thickness of AlGaN layer (listed in Table 1), which could induce the incomplete coalescence of island in the growth process [29,30]. Thus, surface roughness of the four samples obtained by SE fitting as shown in Table 1 are in accordance with the SEM results.

The refractive index (n) and the extinction coefficient (k) of the four samples with different Al content in the wavelength range of 195–1650 nm at 300 K can be extracted by SE fitting, as shown in Fig. 3. The sharp peaks in the spectra of refractive index are due to the excitonic transitions at the bandgap edge, indicating that the AlGaN samples are transparent in the wavelength region of the decrease of refractive index. As the Al content increases, the peak of refractive index spectra shifts toward higher energy (blue shift), inducing the decrease of refractive index value in the same wavelength point of the transparent region, which is in accordance with the expected physical phenomena [11,18,31]. Furthermore, it is observed from the inset of Fig. 3(a), for Al contents x = 0.47 and x = 0.60, the values obtained in this work are similar to those previously reported from Ref. [31] and the maximum deviation is within 0.8%. Combined with the data in Ref. [18] (x = 0.19 and x = 0.675), the overall refractive indices also present a decrease with the increasing Al content in the transparent region. It's noted that, the refractive index values of $Al_xGa_{1-x}N$ (x = 0.75) sample in the transparent region are unusually much smaller than the ones of $Al_xGa_{1-x}N$ (x = 0.60) sample and the ones of $Al_xGa_{1-x}N$ (x = 0.675) in Ref. [18], which could be attributed to the pits on the surface [21] and the relatively thinnest epi-layer of this set of samples. The reduction of refractive index value with the decreasing film thickness has been reported by other authors [21,32,33].

The optical absorption coefficient (α) can be expressed by using Eq. (1), and the energy bandgap can be estimated by using Eq. (2) for direct band gap materials [9,25].

$$\alpha = 4\pi k/\lambda, \tag{1}$$

$$(\alpha(\hbar\omega))^2 = \begin{cases} C(\hbar\omega - E_g) & \hbar\omega \geq E_g, \\ 0 & \hbar\omega < E_g, \end{cases} \tag{2}$$

Here λ is the wavelength, C is a constant. Thus, the values of the bandgap (E_g) can be determined at the point of $(\alpha(\hbar w))^2 = 0$ by linear fit close to the absorption edge [25], as demonstrated in Fig. 4.

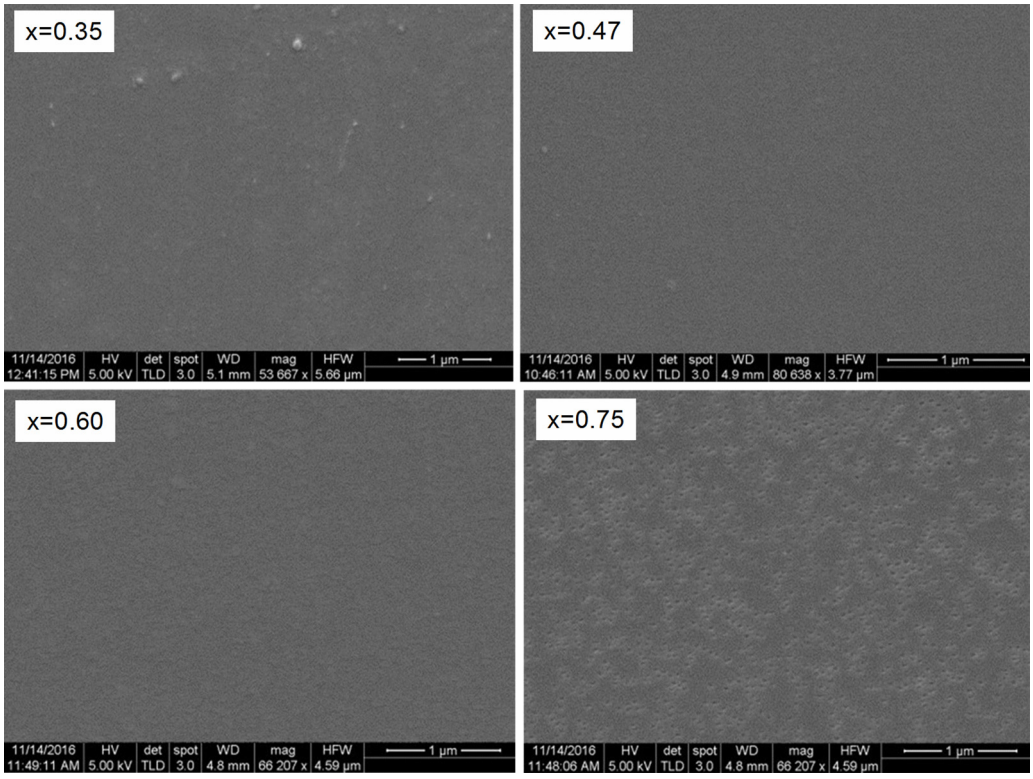

Fig. 2. SEM micrographs for the $Al_xGa_{1-x}N$ samples with x = 0.35, 0.47, 0.60, 0.75, respectively.

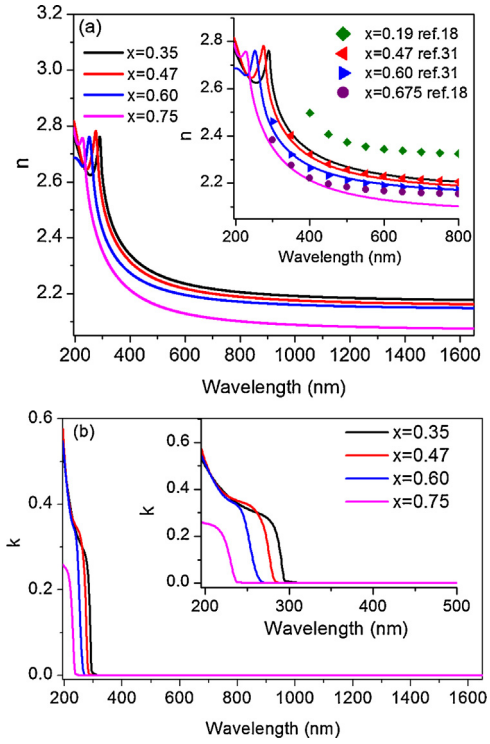

Fig. 3. Optical constants as a function of wavelength for $Al_xGa_{1-x}N$ (x = 0.35, 0.47, 0.60, 0.75) at 300 K. (a) The fitted refractive indices (n). The inset displays a comparison of the fit results from Ref. [18], Ref. [31] and from this work below the wavelength of 800 nm. (b) The fit extinction coefficients (k). The inset shows the spectra in the wavelength range of 195–500 nm.

Fig. 5 shows the PL spectra at 300 K for these four samples, and the transition bandgap energy can be estimated by fitting the spectra near the emission peaks by the Gaussian functions. It is noticed that the PL intensity for the samples of x = 0.35 and 0.75 are much lower than the others, which can be explained by the poor surface morphologies and crystal qualities of these two samples.

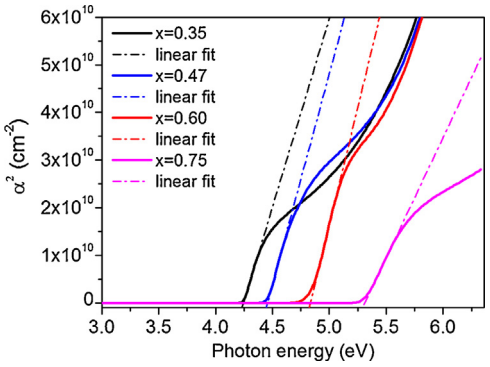

Fig. 4. The square of the absorption coefficient (α^2) vs. photon energy for different Al contents of $Al_xGa_{1-x}N$ samples at 300 K.

Fig. 6 displays the room temperature bandgap obtained by SE fitting and PL measurements, compared with the calculated values following the phenomenological quadratic dependence on the Al content:

$$E_g(Al_xGa_{1-x}N) = xE_g(AlN) + (1-x)E_g(GaN) - bx(1-x), \quad (3)$$

where the bowing parameter b = 0.82 and the room temperature band gaps of 6.1 eV and 3.45 eV for AlN and GaN are determined by Ref. [31]. It is observed that the bandgap extracted from SE fitting are in excellent agreement with the PL and calculated results at 300 K, and the maximum deviation is 0.8%.

The bandgaps, refractive indices, thickness of layers and surface roughness obtained by SE fitting are in good agreement with

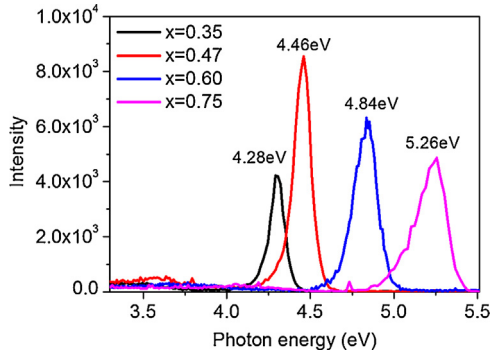

Fig. 5. PL spectra for different Al contents of $Al_xGa_{1-x}N$ samples at 300 K.

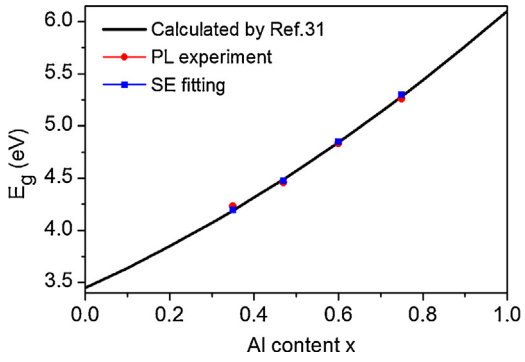

Fig. 6. Room-temperature bandgap (E_g) of $Al_xGa_{1-x}N$ by SE fitting and PL experiment vs. Al content x. The solid line represents the calculated results from Ref. [31].

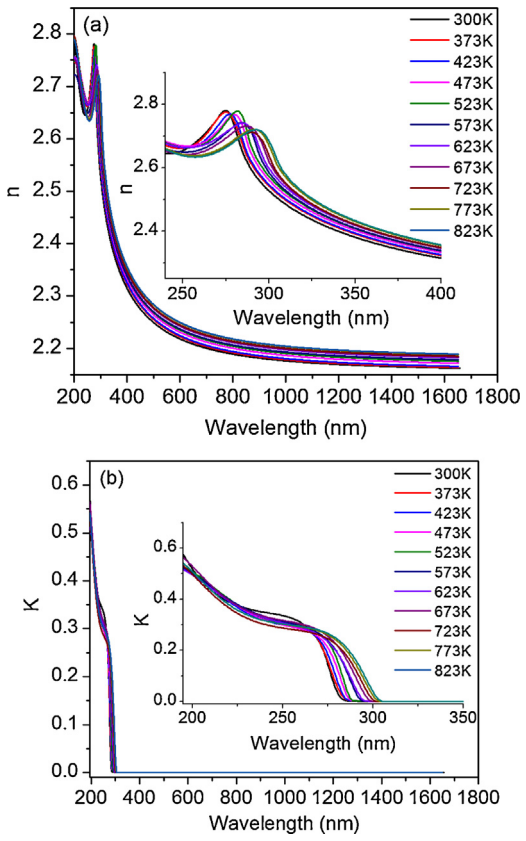

Fig. 7. Fitted optical constants at elevated temperatures (300–823 K) in the wavelength range of 195–1650 nm for $Al_xGa_{1-x}N$ (x = 0.47). (a) The fitted refractive indices (n). The inset shows the spectra in the wavelength range of 240–400 nm. (b) The fitted extinction coefficients (k). The inset shows the spectra in the wavelength range of 195–350 nm.

PL, SEM measurements and the existing literature, which demonstrates the accuracy of the dispersion models used in this work.

4.2. Temperature-dependent modeling and analysis

The fitted parameters of the models at 300 K can be used as the initial values for the fitting procedure at elevated temperature. The temperature dependence of the optical property constants for the sapphire substrate has been omitted in this work, due to almost no temperature-induced deviation of optical constants [11]. The thickness of AlGaN/interface/AlN layers, surface roughness and the dielectric functions of AlGaN and AlN were taken into account for the high-temperature SE fitting. Based on the dispersion models at 300 K, the best-fit results can be obtained at elevated temperatures by adjusting these fitting parameters within reasonable borders.

The fitted thicknesses of every layer for the samples increase slightly at elevated temperatures, and the largest increase of the thickness caused by thermal expansion effect is 0.95% as the temperature rises from 300 to 823 K. For example, the thickness of the epi-layer varies from 775.3 nm to 778.5 nm in the whole temperature range for the $Al_xGa_{1-x}N$ (x = 0.35) sample.

4.3. Dependence of the refractive index on temperature

Fig. 7 shows the fitted refractive indices for $Al_xGa_{1-x}N$ (x = 0.47) in the wavelength range of 195–1650 nm at eleven temperature points from 300 to 823 K. It is observed that the refractive index increases with the increase of temperature in the transparent region due to the red-shift of the refractive index peaks. The changes of refractive index are pronounced in the vicinity of the bandgap. For instance, the refractive index of $Al_{0.47}Ga_{0.53}N$ increases from 2.50 to 2.62 in the wavelength of 305 nm, and increases from 2.16 to 2.19 in the wavelength of 1650 nm with increasing temperature from 300 to 823 K. These results are also in agreement with the previously published ones [4,8,11].

Fig. 8 shows the optical constants extracted by SE fitting for the other three samples at the highest temperature of 823 K, compared with the fitting results at 300 K. It is observed that as the temperature rises, the refractive index increases noticeably stronger in low Al samples than that in high Al samples. For instance, in the wavelength of 1650 nm, the increase of refractive index is 0.029 (from 2.177 to 2.206) for $Al_{0.35}Ga_{0.65}N$, while the increase of refractive index is 0.012 (from 2.075 to 2.087) for $Al_{0.75}Ga_{0.25}N$ with increasing temperature.

The single oscillator approximate Sellmeier equation can be used to describe the SE-derived refractive index spectra in the transparent region [24] for the quantitative analysis:

$$n(\lambda) = \left(1 + \frac{A\lambda^2}{\lambda^2 - B}\right)^{1/2}, \quad (4)$$

where λ is the wavelength (nm), A and B (nm^2) are the fit-determined parameters. The regression fitted A and B at elevated temperatures for the four samples are plotted in Fig. 9. We note that the values of A and B decrease with the increasing Al content, and increase at elevated temperatures. Furthermore, the variation of A with the function of temperature is more noticeable in lower Al content samples than that of higher Al content samples. A quadratic equation can be employed to fit and describe the temperature-dependent A and B, as shown in Fig. 9. Thus, an analytical expression n (λ, T) can be obtained from the quantitative analysis, and the

Table 3
The fit parameters in Eq. (5) for different Al content.

Al content x	A_0	A_1 ($\times10^{-5}$ K^{-1})	A_2 ($\times10^{-7}$ K^{-2})	B_0 (nm^2)	B_1 (nm^2 K^{-1})	B_2 ($\times10^{-3}$ nm^2 K^{-2})
0.35	3.651 ± 0.008	4.03 ± 0.30	1.74 ± 0.03	29103 ± 39	1.21 ± 0.14	1.69 ± 0.12
0.47	3.589 ± 0.007	0.72 ± 0.26	1.98 ± 0.02	28515 ± 94	−0.80 ± 0.35	4.29 ± 0.31
0.60	3.546 ± 0.007	4.63 ± 0.27	0.72 ± 0.02	26133 ± 81	−4.52 ± 0.30	7.25 ± 0.26
0.75	3.281 ± 0.003	0.57 ± 0.11	0.75 ± 0.01	24059 ± 70	−2.72 ± 0.28	6.62 ± 0.23

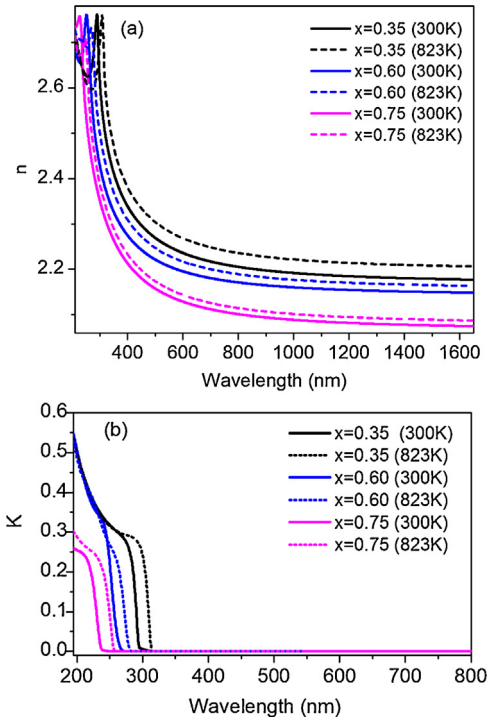

Fig. 8. Fitted optical constants of $Al_xGa_{1-x}N$ (x = 0.35, 0.60 and 0.75) at 300 and 823 K. (a) Refractive indices (n) vs. wavelength. (b) Extinction coefficients (k) vs. wavelength.

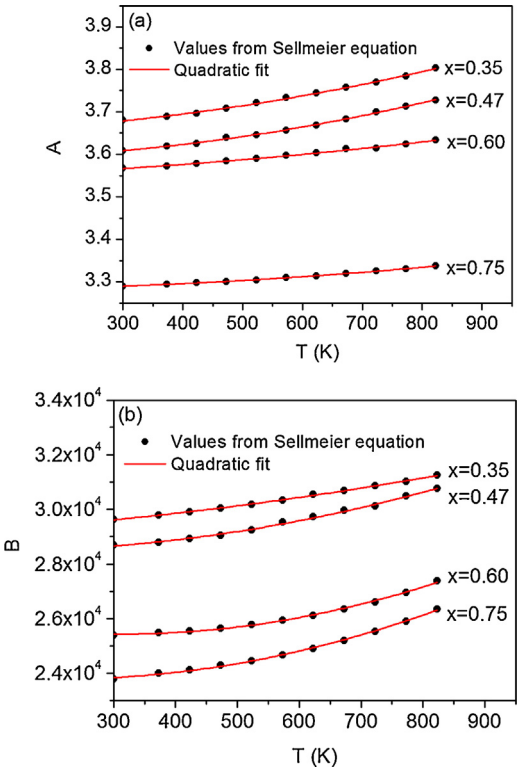

Fig. 9. Plots of A and B in the Sellmeier equation and the quadratic fit for the temperature-dependent A and B.

parameter values in this expression (Eq. (5)) for different Al content are listed in Table 3.

$$\begin{cases} n(\lambda, T) = [1 + \dfrac{A(T)\lambda^2}{\lambda^2 - B(T)}]^{1/2} \\ A(T) = A_0 + A_1 T + A_2 T^2 \\ B(T) = B_0 + B_1 T + B_2 T^2 \end{cases} \quad (5)$$

4.4. Dependence of the bandgap on temperature

Using the same methods presented in section 4.1, the square of the absorption coefficient (α^2) vs. photon energy in the temperature range of 300 K ≤ T ≤ 823 K for the four samples can be obtained from the SE fitting results and then the optical bandgap can be calculated from the linear fit, as shown in Fig. 10 and Fig. 11. It is clear that, similar to the peaks of refractive index, the absorption edge also shift to the lower energy (red-shift) with rising temperature for all Al composition $Al_xGa_{1-x}N$. This result indicates that the bandgap decreases with the increase of temperature, as shown in Fig. 11. For semiconductors, the reduction of bandgap with increasing temperature is generally due to the lattice thermal expansion and the change in the acoustic and optic phonons involved electron-phonon interactions [9,34]. As the temperature rises, the inter-atomic spacing increases. That is influenced by two factors: the increasing amplitude of the atomic vibrations due to the increased thermal energy, and the thermal expansion. An increased

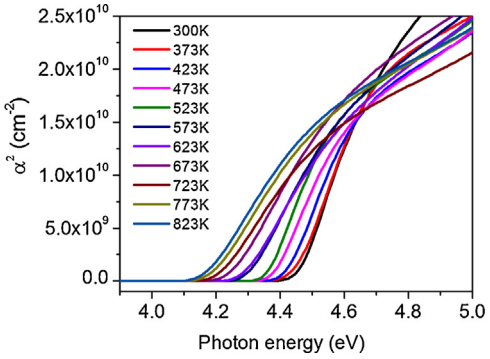

Fig. 10. The square of the absorption coefficient (α^2) vs. photon energy at elevated temperatures (300–823 K) for $Al_xGa_{1-x}N$(x = 0.47) sample.

inter-atomic spacing decreases the potential energy of electrons, which in turn reduces the bandgap energy [35]. According to these principles, high compressive strain also can cause an increase of the bandgap.

Fig. 11 also shows the temperature dependence of E_g reported by Ref. [10]. For the purpose of precise comparison with the results from this work, we only present the temperature-dependent E_g for the $Al_xGa_{1-x}N$ (x = 0.60) sample used in Ref. [10], which is directly obtained by the least squares fit of PL measurements with the Vashni equation. While the temperature-dependent E_g for

Table 4
The fit parameters of a_B and θ of $Al_xGa_{1-x}N$ ($0 \le x \le 1$) *epi*-layers using Eq. (6).

Al content x	a_B(meV)	θ (K)	Temperature range	Techniques	Reference
0	112 ± 6	386 ± 15	290–580	PL	[11]
0	158 ± 4	564 ± 20	10–700	PL	[39]
0	158 ± 8	569 ± 19	30–690	SE	[40]
0.35	210 ± 10	691 ± 26	300–823	SE	This work
0.47	260 ± 15	735 ± 31			
0.60	313 ± 18	790 ± 34			
0.75	475 ± 12	980 ± 17			
1	670 ± 40	1000 ± 50	10–800	PL	[39]

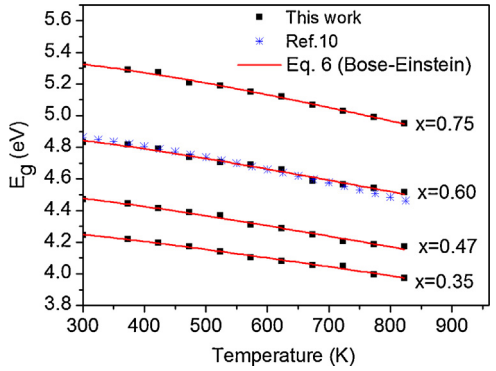

Fig. 11. Temperature dependence of the bandgap energies between 300 and 823 K for $Al_xGa_{1-x}N$ samples ($0.35 \le x \le 0.75$), compared with the reported results from Ref. [10]. The solid red line represents the best fitting results using Eq. (6).

$Al_xGa_{1-x}N$ (x = 0.35, 0.47, and 0.75) in Ref. [10] should be calculated by combining Eq. (2)–(6) presented in Ref. [10], which can lead to relatively large error, as illustrated in Ref. [36]. It is observed that the values of bandgap in Ref. [10] lie slightly above the one in this work at 300 K, which can be attributed to the different structure and strain of samples between our work and Ref. [10]. The thickness of the $Al_xGa_{1-x}N$ (x = 0.60) epi-layer used in Ref. [10] (1 μm) is larger than the one used in this work (502 nm). The increased thickness of AlGaN epi-layer can enhance the compressive strain, which induce a decrease of the distance of the average inter-atomic, and lead to the increase of the bandgap [8,18]. The dependence of bandgap on thickness has been reported for various semiconductors [21,37,38]. As we can see from Fig. 11, when the temperature increases the reduction of the bandgap are more pronounced in high Al content samples than that in low Al content. From 300 to 823 K, the whole reduction value of E_g is 0.37 eV for x = 0.75 compared with the value of 0.27 eV for x = 0.35. The reason is that the strength of the average electron-phonon interactions in AlN is much stronger than that in GaN [39].

For the further quantitative analysis of temperature-dependent optical bandgap, the phenomenological Bose-Einstein equation can be used to describe the energy bandgap as a function of temperature [36,39]:

$$E(T) = E(0) - 2a_B/[\exp(\frac{\theta}{T}) - 1], \quad (6)$$

where E(0) is the bandgap energy at 0 K, a_B is the strength of the average electron-phononinteraction, and θ is the average phonon temperature.

Using Eq. (6) we can do the least squares fit to the data of our samples, and the fitted values are listed in Table 4. We also list the fitted values for AlN and GaN epi-layers in the similar temperature range from other literature for comparison. The values of a_B and θ for $Al_xGa_{1-x}N$ layers ($0.35 \le x \le 0.75$) in this work are all below the ones for AlN layers and above the ones for GaN layers in the literature, which is in accordance with the physical mechanism and confirm the accuracy of our fitting results. Furthermore, the values of a_B and θ both increase with the increasing Al content, indicating that the electron-phonon interaction is enhanced in AlGaN thin films with high Al content.

5. Conclusion

The influence of Al content ($0.35 \le x \le 0.75$) and temperature ($300\,K \le T \le 823\,K$) on optical properties of epitaxial $Al_xGa_{1-x}N$ layers has been studied with high accuracy by spectroscopic ellipsometry. It has been illustrated that the surface morphologies and crystal qualities of the samples with x = 0.47 and 0.60 are better than those with x = 0.35 and 0.75. With increasing temperature, the refractive indices increase in the transparent region, and the optical bandgap values decrease for all studied samples. The fitted parameters (A and B) of the Sellmeier equation to describe the temperature-dependent refractive index in the transparent spectral range both increase with decreasing Al content and increasing temperatures. The reduction of band gap with temperature is more pronounced for higher Al content, indicating that electron-phonon interaction increases in Al-rich AlGaN films. The quantitative analysis of temperature-dependent refractive index and optical bandgap have been proposed, which enable us to predict the thermo-optic effect and optimize the optical properties of $Al_xGa_{1-x}N$ based high-temperature power device at elevated ambient or self-heating temperature up to 823 K.

Acknowledgments

We acknowledge the funding supports from the National Natural Science Foundation of China (Grant Nos. 61367004 and 61504030), the Guangxi Science Foundation (Gant No. 2013GXNSFFA019001), and US National Science Foundation Support (Grant No. CMMI-1351817).

References

[1] B. Kucukgok, N. Lu, I.T. Ferguson, S.C. Wang, X. Zhang, Z.C. Feng, Structural and optical analyses of $Al_xGa_{1-x}N$ thin films grown by metal organic chemical vapor deposition, Jpn. J. Appl. Phys. 54 (2015) 02BA05.
[2] B. Albrecht, S. Kopta, O. John, L. Kirste, R. Driad, K. Kohler, M. Walther, O. Ambacher, AlGaN ultraviolet a and ultraviolet C photodetectors with very high specific detectivity D^*, Jpn. J. Appl. Phys. 52 (2013) 08JB28.
[3] L. Sun, J. Chen, J. Li, H. Jiang, AlGaN solar-blind avalanche photodiodes with high multiplication gain, Appl. Phys. Lett. 97 (2010) 191103.
[4] N. Watanabe, T. Kimoto, J. Suda, The temperature dependence of the refractive indices of GaN and AlN from room temperature up to 515 °C, J. Appl. Phys. 104 (2008) 106101.
[5] M.D. Vittorio, B. Potì, M.T. Todaro, M.C. Frassanito, A. Pomarico, A. Passaseo, M. Lomascolo, R. Cingolani, High temperature characterization of GaN-based photodetectors, Sens. Actuators A 113 (2004) 329–333.
[6] C. Fleury, M. Capriotti, M. Rigato, O. Hilt, J. Würfl, J. Derluyn, S. Steinhauer, A. Köck, G. Strasser, D. Pogany, High temperature performances of normally-off p-GaN gate AlGaN/GaN HEMTs on SiC and Si substrates for power applications, Microelectron. Reliab. 55 (2015) 1687–1691.
[7] A.Y. Hudeish, C.K. Tan, A.A. Aziz, Z. Hassan, A chemical sensor based on AlGaN, Mater. Sci. Forum 517 (2006) 33–36.
[8] D. Brunner, H. Angerer, E. Bustarret, F. Freudenberg, R. Höpler, R. Dimitrov, O. Ambacher, M. Stutzmann, Optical constants of epitaxial AlGaN films and their temperature dependence, J. Appl. Phys. 82 (1997) 5090–5096.

[9] S. Sohal, W. Feng, M. Pandikunta, V.V. Kuryatkov, S.A. Nikishin, M. Holtz, Influence of phonons on the temperature dependence of the band gap of AlN and $Al_xGa_{1-x}N$ alloys with high AlN mole fraction, J. Appl. Phys. 113 (2013) 043501.
[10] N. Nepal, J. Li, M.L. Nakarmi, J.Y. Lin, H.X. Jiang, Temperature and compositional dependence of the energy band gap of AlGaN alloys, Appl. Phys. Lett. 87 (2005) 242104.
[11] U. Tisch, B. Meyler, O. Katz, E. Finkman, J. Salzman, Dependence of the refractive index of $Al_xGa_{1-x}N$ on temperature and composition at elevated temperatures, J. Appl. Phys. 89 (2001) 2676–2685.
[12] J. Petalas, S. Logothetidis, S. Boultadakis, Optical and electronic-structure study of cubic and hexagonal GaN thin films, Phys. Rev. B 52 (1995) 8082–8091.
[13] Martin Feneberg, María Fátima Romero, Benjamin Neuschl, Klaus Thonke, Marcus Röppischer, Christoph Cobet, Norbert Esser, Matthias Bickermann, Rüdiger Goldhahn, Temperature dependent dielectric function and reflectivity spectra of nonpolar wurtzite AlN, Thin Solid Films 571 (2014) 503–506.
[14] L. Siozade, S. Colard, M. Mihailovic, J. Leymarie, A. Vasson, N. Grandjean, M. Leroux, J. Massies, Temperature dependence of optical properties of h-GaN films studied by reflectivity and ellipsometry, Jpn. J. Appl. Phys. 39 (2000) 20–25.
[15] N.V. Edwardsa, S.D. Yoo, M.D. Bremser, M.N. Horton, N.R. Perkins, T.W. Weeks Jr., H. Liu, R.A. Stall, T.F. Kuech, R.F. Davis, D.E. Aspnes, Spectroscopic ellipsometry and low-temperature reflectance: complementary analysis of GaN thin films, Thin Solid Films 313 (1998) 187–192.
[16] Y. Koide, H. Itoh, M.R.H. Khan, K. Hiramatu, N. Sawaki, I. Akasaki, Energy band-gap bowing parameter in an $Al_xGa_{1-x}N$ alloy, J. Appl. Phys. 61 (1987) 4540–4543.
[17] Q.H. Li, D. Zhu, W. Liu, Y. Liu, X.C. Ma, Optical properties of Al-doped ZnO thin films by ellipsometry, Appl. Surf. Sci. 254 (2008) 2922–2926.
[18] N. Antoine-Vincent, F. Natali, M. Mihailovic, A. Vasson, J. Leymarie, P. Disseix, D. Byrne, F. Semond, J. Massies, Determination of the refractive indices of AlN GaN, and $Al_xGa_{1-x}N$ grown on (111)Si substrates, J. Appl. Phys. 93 (2003) 5222–5226.
[19] D.E. Aspnes, J. Theeten, F. Hottier, Investigation of effective-medium models of microscopic surface roughness by spectroscopic ellipsometry, Phys. Rev. B 20 (1979) 3292.
[20] S. Adachi, Properties of Semiconductor Alloys: Group-IV, III-V and II-VI Semiconductors, first ed., John Wiley & Sons, West Sussex, 2009.
[21] P. Motamedi, K. Cadien, Structural and optical characterization of low-temperature ALD crystalline AlN, J. Cryst. Growth 421 (2015) 45–52.
[22] C.M. Herzinger, B. Johs, W.A. McGahan, J.A. Woollam, W. Paulson, Ellipsometric determination of optical constants for silicon and thermally grown silicon dioxide via a multi-sample, multi-wavelength, multi-angle investigation, J. Appl. Phys. 83 (1998) 3323.
[23] C.M. Herzinger, B.D. Johs, Dielectric Function Parametric Model and Method of Use, 1998.
[24] G. Yu, H. Ishikawa, T. Egawa, T. Soga, J. Watanabe, T. Jimbo, M. Umeno, Polarized reflectance spectroscopy and spectroscopic ellipsometry determination of the optical anisotropy of gallium nitride on sapphire, Jpn. J. Appl. Phys. 36 (1997) L1029–L1031.
[25] H. Fujiwara, Spectroscopic Ellipsometry Principles and Applications, first ed., John Wiley & Sons, Ltd, West Sussex, 2007.
[26] C. McAleese, M.J. Kappers, F.D.G. Rayment, P. Cherns, C.J. Humphreys, Strain effects of AlN interlayers for MOVPE growth of crack-free AlGaN and AlN/GaN multilayers on GaN, J. Cryst. Growth 272 (2004) 475–480.
[27] Z.X. Qin, H.J. Luo, Z.Z. Chen, T.J. Yu, Z.J. Yang, K. Xu, G.Y. Zhang, Effect of AlN interlayer on incorporation efficiency of Al composition in AlGaN grown by MOVPE, J. Cryst. Growth 298 (2007) 354–356.
[28] V. Siklitsky, New semiconductor materials, Characteristics and Properties. http://www.ioffe.ru/SVA/NSM/Semicond/, (accessed 16.11.15).
[29] J.N. Dai, Z.H. Wu, C.H. Yu, Q. Zhang, Y.Q. Sun, Y.K. Xiong, X.Y. Han, L.Z. Tong, Q.H. He, F.A. Ponce, C.Q. Chen, Comparative study on MOCVD growth of a-Plane GaN films on r-Plane sapphire substrates using GaN AlGaN, and AlN buffer layers, J. Electron. Mater. 38 (2009) 1938–1943.
[30] B.A. Haskell, S. Nakamura, S.P. DenBaars, J.S. Speck, Progress in the growth of nonpolar gallium nitride, Phys. Status Solid B 244 (2007) 2847–2858.
[31] K. Takeuchi, S. Adachi, K. Ohtsuka, Optical properties of $Al_xGa_{1-x}N$ alloy, J. Appl. Phys. 107 (2010) 023306.
[32] Y. Akaltun, M.A. Yıldırım, A. Ateş, M. Yıldırım, The relationship between refractive index-energy gap and the film thickness effect on the characteristic parameters of CdSe thin films, Opt. Commun. 284 (2011) 2307–2311.
[33] E.S.M. Goh, T.P. Chen, C.Q. Sun, Y.C. Liu, Thickness effect on the band gap and optical properties of germanium thin films, J. Appl. Phys. 107 (2010) 024305.
[34] S.G. Choi, T.J. Kim, S.Y. Hwang, J. Li, C. Persson, Y.D. Kim, S.-H. Wei, I.L. Repins, Temperature dependent band-gap energy for $Cu_2ZnSnSe_4$: A spectroscopic ellipsometric study, Sol. Energy Mater. Sol. Cells 130 (2014) 375–379.
[35] Temperature dependence of the energy bandgap. http://ecee.colorado.edu/~bart/book/eband5.htm, (accessed 16.10.23).
[36] V. Kumar, Anita Sinha, U. Farooque, Concentration and temperature dependence of the energy gap in some binary and alloy semiconductors, Infrared Phys. Technol. 69 (2015) 222–227.
[37] M. Ben Rabeh, N. Khedmi, M.A. Fodha, M. Kanzari, The effect of thickness on optical band gap and N-type conductivity of CuInS2 thin films annealed in air atmosphere, Energy Procedia 44 (2014) 52–60.
[38] A. Rahal, S. Benramache, B. Benhaoua, The effect of the film thickness and doping content of SnO2:F thin films prepared by the ultrasonic spray method, J. Semicond. 34 (2013) 093003.
[39] K.B. Nam, J. Li, J.Y. Lin, H.X. Jiang, Optical properties of AlN and GaN in elevated temperatures, Appl. Phys. Lett. 85 (2004) 3489–3491.
[40] T.J. Kim, S.Y. Hwang, J.S. Byun, N.S. Barange, H.G. Park, Y.D. Kim, Temperature dependent dielectric function and the E 0 critical points of hexagonal GaN from 30 to 690 K, AIP Adv. 4 (2014) 027124.